Chemistry & Biology, Vol. 12, 1227–1234, November, 2005, ©2005 Elsevier Ltd All rights reserved. DOI 10.1016/j.chembiol.2005.09.008

Unmodified Cadmium Telluride Quantum Dots Induce Reactive Oxygen Species Formation Leading to Multiple Organelle Damage and Cell Death

Jasmina Lovrić,[1,2] Sung Ju Cho,[1] Françoise M. Winnik,[3] and Dusica Maysinger[1,*]
[1]Department of Pharmacology and Therapeutics
McGill University
3655 Promenade Sir-William-Osler
McIntyre Medical Sciences Building
Room 1314
Montreal, Quebec H3G 1Y6
Canada
[2]Faculty of Pharmacy and Biochemistry
University of Zagreb
Ante Kovačića 1
10 000 Zagreb
Croatia
[3]Faculty of Pharmacy and Department of Chemistry
University of Montreal
Pavillon J. A. Bombardier
C.P. 6128 Succursale Centre-Ville
Montreal, Quebec H3C 3J7
Canada

Summary

Quantum dots (QDs) are luminescent nanoparticles with unique optical properties that have been exploited for single-cell and whole-animal imaging. When coated with proteins or biocompatible polymers, QDs are not deleterious to cells and organisms. However, when QDs are retained in cells or accumulated in the body for a long period of time, their coatings may be degraded, yielding "naked" QDs. Here, we show that "naked" QDs induce damage to the plasma membrane, mitochondrion, and nucleus, leading to cell death. Reactive oxygen species (ROS) are important players in mediating QD-induced cellular damage. QD-induced cytotoxicity can be reduced or even eliminated without covalent binding of protective agents to the QD surface. Results from these studies suggest the critical role of several subcellular compartments in QD-induced cytotoxicity and point toward multiple molecular targets in nonclassical apoptosis.

Introduction

Various engineered nanoparticles have become important tools in biomedical research, and, among them, semiconductor nanocrystals called quantum dots (QDs) show the greatest promise [1, 2]. Their unique optical properties make them advantageous probes for multicolor and long-term live-cell imaging [3–6]. Moreover, QDs are also excellent candidate agents for in vivo diagnostic imaging [7–13].

Despite the advantages of QDs over fluorescent dyes, the toxicity of QDs has not been thoroughly examined. While mostly neglected, or mainly attributed to the toxic effects of heavy metals leaching from the nanoparticles, QD toxicity may also derive from their intrinsic properties, such as size and surface chemistry. More importantly, since QDs are efficient energy donors [14, 15], they could transfer energy to nearby oxygen molecules, inducing the generation of reactive oxygen species (ROS), in turn leading to cell damage or death [16]. In fact, cadmium selenide (CdSe) QDs have been shown to generate singlet oxygen in vitro [17]. Singlet oxygen and/or hydroxyl free radicals photogenerated upon irradiation of QDs were also suggested as the most likely species responsible for the plasmid DNA nicking taking place immediately upon irradiation of DNA in the presence of QDs [18]. Generation of free radicals and DNA damage were observed even without exposure to light, suggesting that the mechanism of DNA nicking is not a simple photo-induced free radical process.

Even though some reports show strong evidence for the survival of cells loaded with QDs for weeks without alteration in cell growth and division [19], other studies indicate that high concentrations of QDs (>5×10^9 QDs/cell) can impair embryonic development [20]. Polymer-coated QDs are accumulated in mouse bone marrow, spleen, and liver for at least 4 months after systemic administration [21]. QD toxicity can be altered by surface modifications [22, 23], suggesting that reactive surfaces may play a role in QD-induced cytotoxicity. Moreover, it has been shown that exposure of the CdSe core to oxidative environments causes the decomposition and desorption of Cd^{2+} ions [22, 24], well known potent toxins.

In this study, we have explored green, mercaptopropionic acid (MPA)-coated cadmium telluride (CdTe) QDs synthesized in water. Deprotonated thiols (thiolates) are most often used as ligands to stabilize quantum dots in solution, and MPA is among the smallest ones [25]. It seems that the chain length of the stabilizing ligand is an important factor controlling the stability of QDs: longer chains enhance the stability. Aggregation of QDs in solution takes place when the stabilizing ligands are removed from the nanocrystal surface via protonation [26] or, possibly, photooxidation [25]. We cannot exclude the possibility that similar processes may occur during in vitro or in vivo imaging, depending on the subcellular localization of the QDs and the local pH and redox environment they encounter. Protein or polymer QD coatings could be degraded in vivo, yielding exposed inorganic cores. Such unprotected QDs could represent a hazard for long-term use of QDs.

As a cellular model, we selected a human breast cancer cell line (MCF-7) because they are frequently used in cancer research and mechanisms involved in cell death were well studied. In vivo imaging and phototherapy with QDs have been proposed as highly sensitive, noninvasive means for early cancer diagnosis and treatment. A prerequisite for such applications is the long-term safety of QDs.

The aim of this study was to investigate the mechanisms contributing to cellular toxicity of surface-unprotected CdTe QDs in MCF-7 cultures. The investigation reveals that CdTe QDs induce cell death by nonclassical

*Correspondence: dusica.maysinger@mcgill.ca

apoptosis initiated by reactive oxygen species detectable in live cells.

Results

QDs Trigger Plasma Membrane, Mitochondrial, and Nuclear Damage in MCF-7 Cells

QDs have been shown to induce a decrease in cell viability, which depends on the type of QDs and on the experimental conditions [22, 23, 27, 28]. Subcellular organelles of dying cells manifest alterations in their morphology and function. They sense and respond to stressful stimuli, leading to adaptation or cell death [29]. To examine QD-triggered damage of cells on the subcellular level, we used specific dyes to assess the integrity of plasma membrane, mitochondrion, and nucleus.

Plasma membrane damage was assessed by using propidium iodide (PI), a red fluorescent nuclear stain that cannot enter cells with intact plasma membranes (Figure 1A). The number of PI-positive cells is increased after 12 hr upon treatment with QDs (16.4% PI-positive cells), and it is further increased after 24 hr of treatment (32% for QD-treated versus 4.3% for controls).

Under stressful conditions, the network of elongated mitochondria is disintegrated and transformed into vesicular punctiform mitochondria [30]. The effect of QDs on mitochondrial morphology was analyzed by using MitoTracker Deep Red 633, which selectively stains these organelles. In the absence of QDs, mitochondria are elongated, whereas short, round mitochondria are aggregated at the perinuclear region after 24 hr in the presence of QDs (Figure 1B and Figure S1; see the Supplemental Data available with this article online).

Nuclear morphology is an indicator of the health status of the cell [31]. Staining the nuclei with Hoechst 33342 revealed shrinkage and deformation of nuclei with chromatin aggregation, indicating nuclear damage induced by QD after 24 hr (Figure 1C).

The reduction of MTT (3-(4,5-dimethylthiazol-2-yl)-2,5-diphenyl tetrazolium bromide) to formazan, a measure of cell metabolic activity, was decreased in a dose-dependent manner by QD treatment (Figure 1E). Changes in cell number were determined by measuring Hoechst 33342 fluorescence and correlating it with a calibration curve of a known number of cells. At concentrations of 1 and 5 μg/ml, QDs did not induce cell loss (104.8% ± 5.2% and 97.6% ± 4.8% of control cells, respectively), but, at these concentrations, a decrease in cell metabolic activity was detected. However, at the highest concentration of QDs (10 μg/ml), cell loss was evident (only 64.3% ± 2.6% cells remained). A decrease in the metabolic activity was already observed 4 hr after QD treatment (10 μg/ml, 79.1% ± 1.2% of control cells). At the same time point, cell loss did not yet occur (98.9% ± 4.4% of control cells).

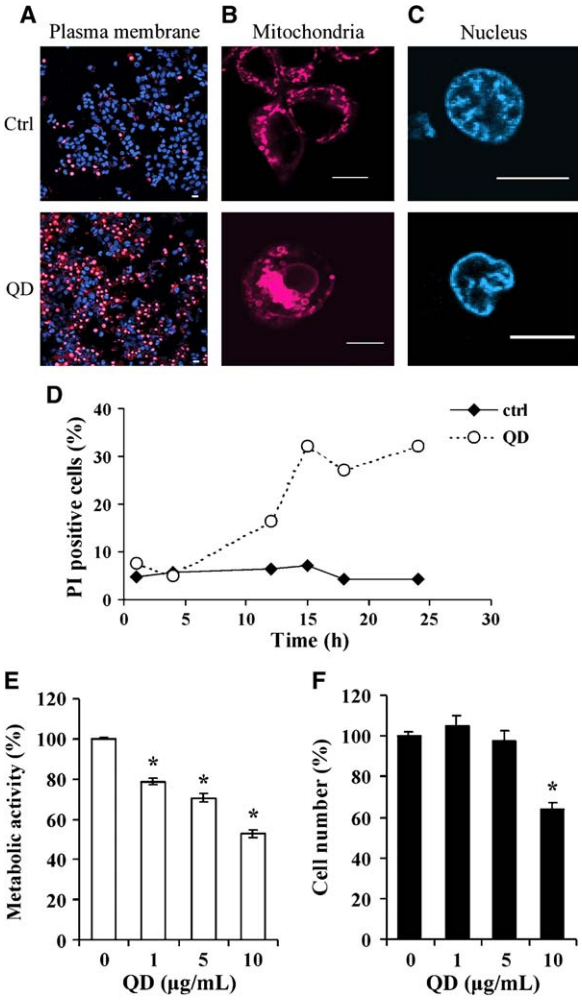

Figure 1. QDs Induce Damage to Plasma Membrane, Mitochondria, and Nucleus

(A) Confocal micrographs of MCF-7 cells double-stained with Hoechst 33342 (10 μM) and PI (7.5 μM) 15 hr after QD treatment (10 μg/ml).

(B) Mitochondria of MCF-7 cells stained with MitoTracker Deep Red 633 (1 μM) 24 hr after QD treatment (5 μg/ml).

(C) Nucleus of MCF-7 cells stained with Hoechst 33342 (10 μM) 24 hr after QD treatment (5 μg/ml).

(D) Quantification of cells with plasma membrane damage (PI positive) as a percentage of the total number of Hoechst-stained cells after QD treatment (10 μg/ml).

(E) The metabolic activity of MCF-7 cells exposed to QDs is decreased in a concentration-dependent manner ($p < 0.001$, $F_{3,39} = 121.496$). Cells were incubated with QDs for 24 hr.

(F) After 24 hr, cell loss occurs when MCF-7 cells are incubated with the highest concentration of QDs (10 μg/ml, $p < 0.001$, $F_{3,35} = 18.602$).

For (E) and (F), data represent mean ± SEM for four and three independent experiments, respectively. The scale bar represents 10 μm. *, $p < 0.001$ as determined with 1-way ANOVA followed by a post-hoc Dunnett's test.

QD-Induced Cell Death Is Caspase-Independent

Caspase activation is often a critical event in classical apoptosis aside from the morphological changes during the apoptosis [32]. MCF-7 cells do not express caspase-3, main effector caspase, but they do express other members of the caspase family. It was shown that apoptosis in MCF-7 cells proceeds via sequential activation of caspase-9, -7, and -6 [33]. So, if QDs induce classical apoptosis, a caspase inhibitor should be able to prevent cell death. We therefore used Z-VAD, a broad caspase inhibitor, to test this hypothesis. Z-VAD (tested in three different concentrations: 10, 30, and 50 μM) was ineffective when MCF-7 cells were incubated with QDs (5 or 10 μg/ml, 24 hr). Z-VAD failed to prevent both a decrease in

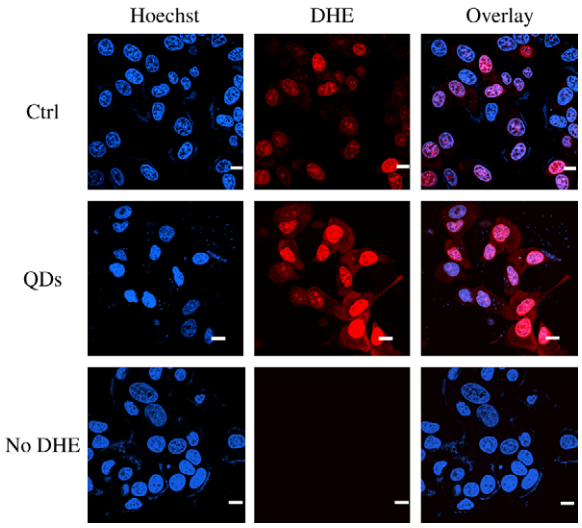

Figure 2. QDs Induce Generation of Reactive Oxygen Species

MCF-7 cells were double stained with DHE (10 μM) and Hoechst 33342 (10 μM) 4 hr after QD treatment (see Experimental Procedures). Confocal micrographs of control cells and QD-treated cells exposed to both dyes, and cells treated with QDs, but not stained with DHE. The scale bar represents 10 μm.

metabolic activity and cell number, as assessed by MTT and Hoechst assay, respectively.

QDs Induce Generation of Reactive Oxygen Species

The generation of excess reactive oxygen species (ROS) causes the modification and damage of cellular proteins, lipids, and DNA, and it can subsequently lead to cell death. To investigate oxidative stress produced by QDs, we used dihydroethidium (DHE). DHE is oxidized by ROS to ethidium, which intercalates with cellular DNA, yielding bright red, fluorescent nuclear staining. Using confocal microscopy, we observed ROS production after 4 hr of QDs exposure in culture medium. Very little fluorescence from ethidium was detected in control cells (Figure 2). However, a significant increase in fluorescence was detected in QD-treated cells (Figure 2 and Figure S2).

NAC Prevents QD-Induced Cellular Damage

Our previous studies demonstrated the effectiveness of antioxidants in preventing the decrease in cell viability by cysteamine-stabilized QDs [28]. N-acetylcysteine (NAC), a strong antioxidant containing a mercapto group, provided complete protection against QD-induced stress. We therefore examined whether the protective effect of NAC was due to the scavenging of ROS after QD treatment. Indeed, NAC (4 mM) prevented QD-induced oxidation of DHE (Figures 3A and 3B and Figure S2). Upon 1, 4, and 24 hr exposure to QDs, cells treated with QDs only displayed bright red, fluorescent nuclei, whereas cells treated with QDs and NAC showed very weak nuclear staining. NAC preserved the normal mitochondrial morphology (Figure 3C) and partially prevented their functional impairment (Figure 3D). However, NAC was very effective in reducing cell loss (Figure 3E).

QD Treatment Leads to a Reduction of Cytochrome c Concentration in Mitochondria

The subcellular distribution of certain proteins changes upon the introduction of stressful stimuli [34]. The

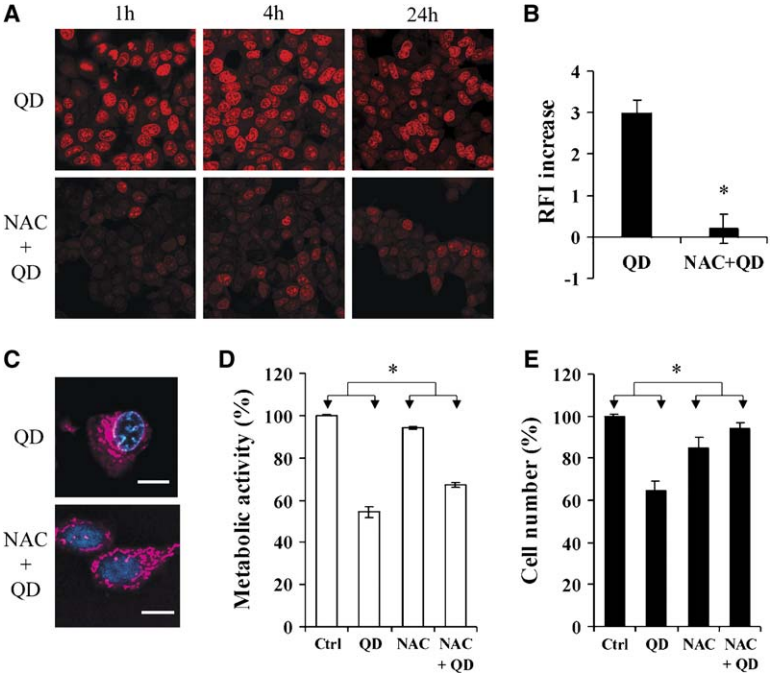

Figure 3. NAC Reduces QD Induction of ROS and Cellular Damage

(A) Confocal micrographs of DHE-stained cells treated with QDs only (10 μg/ml) and QDs in the presence of NAC (4 mM) after 1, 4, and 24 hr.

(B) Semiquantitative analysis of ethidium fluorescence intensity 4 hr after QD treatment. Relative fluorescence intensity (RFI) was divided by the number of cells per field. Results are expressed as an increase of RFI compared to nontreated control cells ($p < 0.05$ as determined by a Student's t test).

(C) Mitochondria stained with MitoTracker Deep Red 633 (1 μM) 24 hr after QD treatment (5 μg/ml) in the absence and presence of NAC (2 mM).

(D) Metabolic activity of cells treated with QD (10 μg/ml) in the presence and absence of NAC (4 mM), and respective controls as measured by an MTT assay. The significant interaction between NAC and QDs was determined by 2-way ANOVA ($p < 0.001$, $F_{1, 32} = 40.365$).

(E) Number of cells 24 hr after QD treatment (10 μg/ml) in the absence and presence of NAC (4 mM) as measured by Hoechst assay. The significant interaction between NAC and QDs was determined by 2-way ANOVA ($p < 0.001$, $F_{1, 32} = 78.625$).

In (B), (D), and (E), data represent mean ± SEM for two, four, and three independent experiments, respectively. The scale bar represents 10 μm.

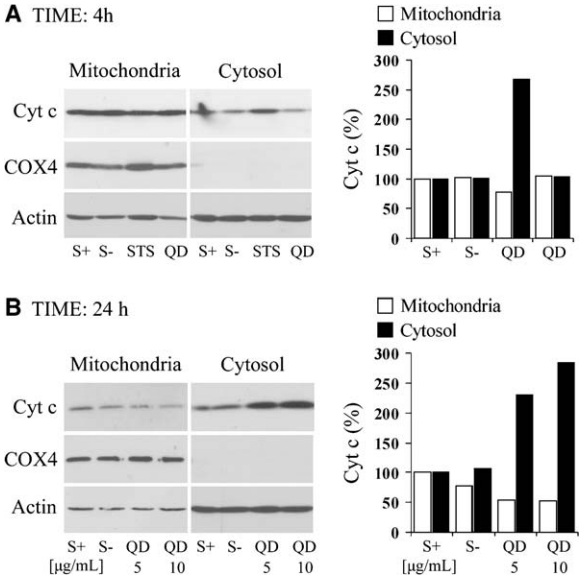

Figure 4. QD Treatment Leads to a Reduction of Cytochrome c Concentration in Mitochondria

(A) Immunoblot analysis of cytochrome c, COX-4, and actin in cytosolic and mitochondrial-enriched fractions 4 hr after QD treatment (left). Semiquantitative data from densitometric analysis of cytochrome c in mitochondria and cytosol (right; three independent experiments). [QD] = 10 μg/ml; [STS] = 2.5 μM.

(B) Immunoblot analysis of cytochrome c, COX-4, and actin in mitochondrial and cytosolic fractions 24 hr after QD treatment (left), and semiquantitative data of the immunoreactive bands (right). COX-4 was used as a control for the fractionation efficiency and for equal loading of proteins in mitochondrial fractions. Actin was used as a control for equal loading of proteins in cytosolic fractions.

intermembrane space of mitochondria harbor proteins that are lethal to the cells once released into cytosol. One such protein is cytochrome c, which in the cytosol plays the role of potent amplifier of apoptotic signals [35]. To investigate the involvement of cytochrome c in QD-mediated cell death, we isolated enriched mitochondrial and cytosolic fractions. Staurosporine (STS), a potent inducer of cytochrome c release and apoptotic cell death [36, 37], was used as a positive control for assessing mislocation of cytochrome c. Cytochrome c release was assessed by Western blotting at two time points, after 4 hr and after 24 hr. After 4 hr, cytochrome c release from mitochondria was significantly enhanced in the cytosol of cells treated with STS (2.5 μM), but not in the cytosol of cells deprived of serum (S− cells) or cells treated with QDs (10 μg/ml) (Figure 4A). However, after 24 hr, QDs (5 and 10 μg/ml) caused cytochrome c release from mitochondria (Figure 4B). The intensity of the cytochrome c immunoreactive band corresponding to S− cells was reduced by 20% compared to cells grown in serum-containing medium (S+), whereas QDs (5 and 10 μg/ml) led to a greater loss of cytochrome c (>40%) with concurrent and significant augmentation in the cytosolic fraction. The mitochondrial loss of cytochrome c was confirmed by using an ELISA assay. The concentration of cytochrome c in mitochondria after a 24 hr QD presence in the cell culture was 424 ng/ml, whereas, in untreated controls, this concentration was 502 ng/ml. However STS (1 μM) induced the most pronounced decrease in cytochrome c concentration (cytochrome c concentration was only 329 ng/ml).

Discussion

Results from this study show that: (1) unmodified CdTe QDs induce damage to plasma membrane, mitochondrion, and nucleus of MCF-7 cells; (2) QD-induced cellular damage is mediated by ROS and can be prevented by treatments with antioxidants; (3) mitochondria release cytochrome c upon the exposure of MCF-7 cells to QDs.

In this study, we have employed green mercaptopropionic (MPA)-coated CdTe quantum dots (2r = 2 nm). The synthesis and properties of QDs employed were originally described by Gaponik et al. [38]. CdTe nanocrystals analyzed by X-ray diffraction and transmission electron microscopy show CdTe cubic crystals, and the EXAFS studies suggested the chemical formula $(Cd_{54}Te_{32}[SCH2CH2COOH]_{52})^{8-}$ and the formation of small aggregates (clusters). Light sensitivity (photochemical stability) of CdTe colloids is strongly dependent on the presence of oxygen and free stabilizer molecules in solution [38]. In oxygen-saturated solutions, photodegradation of CdTe nanoparticles proceeds much faster (>20-fold) than under airless conditions. The photostability of all kinds of thiol-capped CdTe nanocrystals in the solid state is relatively high and independent of the nature of the stabilizer [38]. In this study, QDs were stabilized by MPA. Loss of MPA could occur upon exposure of the QD surface to the cellular environment, possibly leading to oxidation of the inorganic core, release of Cd^{2+}, and QD aggregation. These phenomena may cause enhanced QD cytotoxicity, as previously reported [22]. Hoshino et al. reported that QD toxicity also depends on the methodology employed to purify QDs and to remove the excess reactants (such as MPA) and the by products [23]. In fact, Hoshino et al. point out that, even after QD purification, toxicity cannot be fully eliminated. Imaging of unmodified CdTe QDs is difficult due to their low photoluminescence; however, despite this low photoluminescence, these QDs can be harmful to the cells. Different surface molecules provide a different degree of protection, and they act as a barrier to oxygen, protons, or hole traps. Generally, nanocrystals are less toxic when their surfaces are better protected.

The subcellular organelles are points of damage sensing, and, depending on the extent of damage, cells adapt, repair, or undergo cell death. Our experiments show that QD treatment leads to plasma membrane damage, as assessed by PI. The number of PI-stained cells increases with time, and, upon a 15 hr exposure to QD, there is maximal damage (Figures 1A and 1D). A loss of plasma membrane integrity is considered an early event in necrosis and a late event in apoptosis. Mitochondrial membrane permeabilization is the point of convergence of numerous cell death signals and, together with caspase activation, it is considered to be the central executioner in apoptosis [29]. Mitochondria are organelles that are very sensitive to QD-induced stress. Mitochondrial function is impaired upon cell exposure to very low QD concentrations (Figure 1E) and soon after QD treatment. QDs also induced disintegration of the

tubular mitochondrial network and aggregation of mitochondria in the perinuclear region (Figure 1B and Figure S1), phenomena characteristic of apoptotic cell death [30, 39]. Nuclear condensation with DNA fragmentation is a mark of apoptotic cell death, whereas, in necrosis, nuclei are swollen. Nuclei in cells with QD-induced damage to the plasma membrane did not show prominent swelling, but rather shrinkage and deformation (Figure 1C). Due to the lack of caspase-3, the main effector caspase in apoptosis, cell death in MCF-7 sets in without oligonucleosomal DNA fragmentation [40]. We investigated the possible role of other caspases in QD-induced cell death by pharmacological manipulations. A broad caspase inhibitor, Z-VAD, failed to prevent QD-induced cell death, suggesting that the cell death is caspase-independent. Similarly, QD-induced cell death in PC12 cells, which do express caspase-3, appears to be caspase-independent (unpublished data). Apoptosis-like cell death modes characterized by less compact/complete chromatin condensation have been described, and cell death that occurs without caspase activation falls into this category [31, 41]. Tumor necrosis factor-induced death of MCF-7 cells induces similar changes in nuclear morphology [31]. Moreover, there is necrosis-like cell death that is the result of active cellular processes, and it can be inhibited by oxygen-radical scavengers [42]. Cell death in the presence of caspase inhibition is a subgroup of this necrosis-like cell death [43]. Taken together, these findings suggest that QD-induced cell death in MCF-7 cultures is not classical necrosis or classical apoptosis.

Reactive oxygen species (ROS) are known to mediate cell death in a variety of cell types. Green and Howman reported the production of ROS by CdSe/ZnS QDs in the presence and absence of light [18]. The mechanism of ROS formation in the absence of light is not clear. However, ROS can be formed in an aqueous medium (e.g., cell culture medium), particularly in the presence of exogenous oxygen, since the medium is supplied by CO_2/O_2. Although we did not intentionally expose cells to the light or use CdSe/ZnS QDs, a minimal exposure of CdTe QDs to visible light during solution preparation, inspection of the cells by an inverted microscope, and cell treatments could have initiated ROS formation in aqueous medium kept in a CO_2/O_2 environment.

Results from our confocal microscopy studies show evidence of ROS formation upon QD treatment. When ROS overcome the cellular antioxidant defense system, cells undergo oxidative stress. Results of this stress include modification and damage of cellular components, such as lipids, proteins, and DNA [44, 45]. Oxidation of unsaturated fatty acids results in the generation of lipid peroxides that start a chain reaction leading to oxidation of nearby unsaturated fatty acids that can culminate in the disruption of the plasma membrane and membranes of other cellular organelles. QDs produce ROS in vitro with or without exposure to light [17, 18], and cellular damages observed in our studies are at least in part due to QD-generated ROS. Other synthetic nanomaterials can also induce oxidative stress; for example, uncoated fullerenes induce lipid peroxidation and glutathione depletion [46].

We have demonstrated that the QD generation of ROS is attenuated in the presence of the antioxidant NAC. This antioxidant acts as a direct ROS scavenger and also, indirectly, as an important cellular antioxidant, by triggering an increase in the production of glutathione (GSH) [47]. NAC was shown to maintain mitochondrial oxidative metabolism [48] and to improve cell survival in response to various insults [49, 50]. In our study, NAC abolished ROS-induced oxidation of DHT, as revealed by weak nuclear ethidium staining (Figure 3 and Figure S2). NAC was able to preserve normal mitochondrial morphology after QD treatment. The effect of NAC on the cell metabolic activity could be ascribed to its multiple intra- and extracellular effects: (1) NAC can reduce the concentration of ROS in the cell culture medium; (2) NAC can induce the synthesis of glutathione, the most abundant and effective cellular antioxidant; (3) NAC could improve QD surface passivation, thereby leading to less damage to the mitochondrial redox system. NAC partially prevented functional impairment of mitochondria and almost completely prevented cell loss. These findings suggest that mitochondria are early targets of QD-induced stress and are severely damaged by QDs. The loss of mitochondrial function could be a major reason for QD-induced cell death.

The release of cytochrome c from mitochondria is a central event in apoptotic signaling [51]. A direct role for ROS in cytochrome c release has been suggested, and this role involves the oxidation of cardiolipin, a phospholipid that is important for the association of cytochrome c with the inner mitochondrial membrane [52]. In addition, cytochrome c release can be a consequence of a ROS-induced change in the conformation of adenine nucleotide translocase, a protein involved in mitochondrial permeability transition pore formation [53]. Superoxide (O_2^-) induces cytochrome c release mainly due to the voltage-dependent anion channel-selective permeabilization of the mitochondrial outer membrane [54]. The onset of cytochrome c release depends on the duration and intensity of stressful stimuli. It takes place approximately 4 hr after exposure to strong apoptotic inducers, such as STS [37]. Cytochrome c release did not occur after a 4 hr QD treatment of MCF-7 cells, although a significant amount of ROS was detected. After a 24 hr exposure to QDs, however, the mitochondria of cells exposed to QDs had significantly lost cytochrome c, and prominent immunoreactive bands were detected in cytosolic fractions. Mitochondrial aggregation in budding-like structures, known to precede cytochrome c release [39], was also observed in QD-treated MCF-7 cells. However, the mitochondrial loss of cytochrome c could also be a consequence of oxidative damage of mitochondrial outer membranes.

We propose the mechanism for QD-induced cell death that involves QD generation of ROS in the extracellular environment and intracellularly. These ROS can cause plasma membrane damage and intracellular organelle damage; mitochondria are the first to be affected, and they appear to be the most sensitive organelles (Figure 5).

Significance

Results from these studies suggest the critical role of several subcellular compartments in QD-induced cytotoxicity and point toward multiple molecular targets

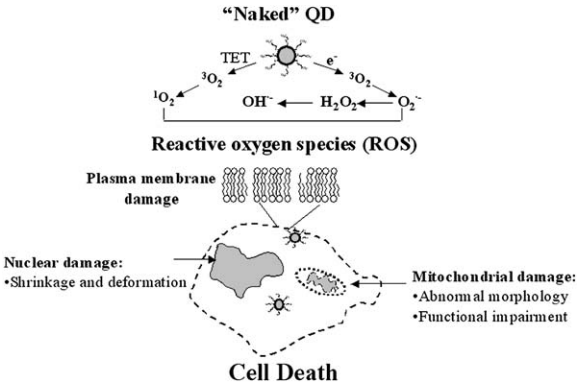

Figure 5. Proposed Mechanism of QD-Induced Toxicity

in nonclassical apoptosis. The mechanism of QD-induced cell death proposed here may take place in cells treated with modified QDs, once they have lost their protective surface coating. Our studies show that "naked" QDs can injure cells, inducing damage to the plasma membrane, mitochondrion, and nucleus. Through electron or energy transfer to the molecular oxygen, QDs can produce reactive oxygen species (ROS) [17]. QD-induced ROS formation and the deleterious effects associated with it therefore can be prevented either by treatment with antioxidants such as N-acetylcysteine (NAC) or by surface modifications. Understanding the molecular mechanisms underlying QD-induced cell death will allow for the development of new QD modifications that could either protect cells (e.g., if used for real-time imaging) or kill cells more efficiently (e.g., if used to complement cancer chemotherapy).

Experimental Procedures

All reagents were purchased from Sigma-Aldrich (Oakville, ON, Canada) unless indicated otherwise. Green mercaptopropionic acid-coated CdTe quantum dots (2r = 2 nm) employed in this study were synthesized as described earlier [38], with a slight modification already reported by our group [28]. Sodium borohydride (1.60 g, 42.3 mmol) was dissolved in water (40 ml) at 0ºC while stirring under N_2. Tellurium powder (2.56 g, 20.1 mmol) was added portionwise, and the mixture was stirred at 0ºC under N_2 for 8 hr, yielding a purple NaHTe solution. The reaction mixture was kept at 4ºC in the dark and was used in the next step. Cadmium perchlorate hydrate (500 μl, 1M aqueous solution) and 3-mercaptopropionic acid (300 μl, 3.9 mmol) were dissolved in water (200 ml). The pH of the solution was adjusted to 10.5 with a 1 M KOH solution prior to addition of an aliquot of the NaHTe solution previously prepared (200 μl). The reaction mixture was heated to reflux for 25 min under N_2. The resulting QD solution was dialyzed against deionized water for 2 hr and concentrated by using a rotary evaporator. QDs were collected by centrifugation and purified by size-selective precipitation.

Cell Culture Conditions, QD, and Drug Treatments

Human breast cancer cells (MCF-7, American Type Culture Collection [ATCC], Rockville, MD) were maintained as per ATCC recommendations. Cells were cultured (37ºC, 5% CO_2) in RPMI 1640 medium containing 10% fetal bovine serum (FBS) (GIBCO-BRL, Burlington, ON, Canada). RPMI 1640 medium was phenol red-free and contained 1% penicillin-streptomycin. For spectrofluorometric and colorimetric assays, cells were cultured in 24-well plates (Sarstedt, Montreal, QC, Canada) at a density of 10^5 cells/cm^2.

One hour prior to treatments, medium containing serum was aspirated, and cells were washed with serum-free medium. Fresh serum-free medium was added to all wells, except to control cells grown in 10% FBS to account for changes in cell morphology, cell number, and metabolic activity due to the serum withdrawal.

Cells were treated with QDs (5 or 10 μg/ml) for different time periods as specified in individual figure legends. QD solutions (5 or 10 μg/ml) were prepared from the stock (2 mg/ml) by dilution in serum-free cell culture medium. Cells were incubated with QDs for a maximum of 24 hr before biochemical analysis or live-cell imaging.

NAC was dissolved in PBS (400 mM), and was added to the culture medium 2 hr before QDs. Staurosporine (STS, Sigma) and Z-VAD (Calbiochem, San Diego, CA) were dissolved in dimethyl sulfoxide (DMSO). STS (used as a positive control for cytochrome c release in Western blotting experiments) was diluted to a final concentration (1 or 2.5 μM) in serum-free medium. Z-VAD was also diluted to a final concentration (10, 30, or 50 μM) in serum-free medium and was added to the cells 2 hr before QDs. All treatments were done in triplicate or quadruplicate in three or more independent experiments.

MTT Assay

Colorimetric MTT (3-[4,5-dimethylthiazol-2-yl]-2,5-diphenyl tetrazolium bromide, Sigma) assays were performed to assess the metabolic activity of cells treated as described above. After 24 hr of treatment, media were removed and replaced with drug-free, serum-free media (500 μl/well). A total of 50 μl stock MTT (5 mg/ml) was added to each well, and cells were then incubated for 1 hr at 37ºC. Media were removed, cells were lysed, and formazan was dissolved with DMSO. Absorbance was measured at 595 nm by using a Benchmark microplate reader (Bio-Rad, Mississauga, ON, Canada). All measurements were done in triplicate in three or more independent experiments.

Hoechst 33342 Assay for Determination of Cell Number

A calibration curve of Hoechst 33342 (Molecular Probes, Eugene, OR) fluorescence intensity as a function of cell number was created in order to determine the number of cells present after QD treatments. Cells were counted by using a hemocytometer and were diluted in RPMI 1640 medium to obtain samples from 30,000 to 1,000,000 cells. Hoechst 33342 (2 mM) was added to the culture medium (final concentration was 10 μM), and cells were incubated for 30 min at 37ºC. At the end of the incubation period, cells were spun down, washed with phosphate-buffered saline (PBS), and lysed with DMSO. Cell lysates were diluted with PBS, and the fluorescence of the samples and respective controls was measured at λ_{ex} 350 nm and λ_{em} 461 nm by using a Molecular Devices SpectraMax Gemini XS microplate spectrofluorometer. The number of cells present after the treatments with QDs and antioxidants was determined by measuring Hoechst 33342 fluorescence intensity and extrapolating the cell number by using a calibration curve. After the treatments, medium containing drugs and QDs was removed, and cells were washed with serum-free medium. Incubation with Hoechst 33342, washing steps, and fluorescence measurements were all performed the same way as for obtaining a calibration curve. All measurements were done in duplicate in three or more independent experiments.

Laser Scanning Confocal Microscopy

Images were acquired with a Zeiss LSM 510 NLO inverted microscope. Cells were grown on 8-well chambers (Lab-Tek, Nalge Nunc International, Rochester, NY). QDs were added to designated wells, and the cells were incubated for different time periods. Plasma membrane damage was investigated by using propidium iodide (PI, 7.5 μM, 10 min, Molecular Probes; λ_{ex} 535 nm, λ_{em} 617 nm [bound to nucleic acids]). The excitation laser and filter used for PI imaging experiments were HeNe 543 nm and LP 560, respectively. Mitochondria were stained with MitoTracker Deep Red 633 (1 μM, 1 min, Molecular Probes; λ_{ex} 644 nm, λ_{em} 665 nm) and were imaged with an HeNe 633 nm excitation laser and an LP 560 filter. Nuclei were stained with Hoechst 33342 (10 μM, 30 min to 1 hr, Molecular Probes; λ_{ex} 350 nm, λ_{em} 461 nm) and were analyzed by 2-photon imaging (Ti:Sa laser set to pulse at 800 nm and BP 390-465 IR filter). Before imaging, cells were washed with PBS or with serum-free medium. No background fluorescence of cells was detected under the settings used. Images were acquired at resolutions of 512 × 512 and 1024 × 1024. In all of the imaging experiments, the number

of averages was four. Scan size was 146.2 μm × 146.2 μm. Figures were created with Adobe Photoshop.

ROS Imaging

ROS generation was imaged by using dihydroethidium (Molecular Probes) and a Zeiss LSM 510 microscope. Cells were cultured for 24 hr on 8-well chamber slides before treatments. After treatments, cells were washed, and medium was replaced with serum-free medium. Dihydroethidium was dissolved in DMSO (3 mM) and added to the culture medium at a final concentration of 10 μM, and the cells were incubated for 30 min at 37ºC. Cells were washed with PBS, and warmed (37ºC), fresh serum-free medium was added before cells were examined by laser scanning confocal microscopy. The oxidation product of DHE is ethidium, whose fluorescence is enhanced ~10-fold when bound to DNA (λ_{ex} 518 nm, λ_{em} 605 nm). Images were acquired by using an HeNe 514 nm laser and an LP 560 filter under set conditions (detector gain was kept constant throughout the experiment). Collected eight-bit images were transferred into monochrome eight-bit TIF files, and quantification of ethidium fluorescence intensity was performed by using the MCID Elite 7.0 imaging system (Imaging Research, St. Catherine's, ON, Canada). All of the results were expressed as relative values to the untreated cells (controls).

Subcellular Fractionation and Western Blotting

Subcellular fractionation was performed by using the ApoAlert cell fractionation kit (BD Biosciences, Mississauga, ON, Canada) according to the manufacture's instructions. Enriched mitochondrial and cytosolic fractions were diluted with 6× Laemmli sample buffer (0.375 M Tris-HCl [pH 6.8], 12% w/v SDS, 3% v/v glycerol, 0.2% w/v bromphenol blue, 12% β-mercaptoethanol in double distilled water) and boiled for 5 min. A total of 25 μg of proteins of each sample were loaded onto a 15% polyacrylamide gel and were transferred onto a nitrocellulose membrane (Bio-Rad, Mississauga, ON, Canada). Cytochrome c and cytochrome c oxidase subunit IV (COX-4) antibody were provided in the ApoAlert kit and were used at dilutions of 1:1000 and 1:500, respectively. Actin antibody (Chemicon, Temecula, CA) was used at a dilution of 1:1000. Secondary antibodies were purchased from Amersham Biosciences (Baie D'Urfe, QC, Canada). The specific protein bands were detected by using ECL reagent (Amersham Biosciences) and were quantified with the MCID-M4 imaging system (Imaging Research).

Cytochrome c ELISA

The cytochrome c ELISA kit was purchased from Chemicon. The concentration of cytochrome c in mitochondrial fractions was determined according to the manufacturer's instructions.

Statistical Analysis

Data were analyzed by using SYSTAT 10 (SPSS, Chicago, IL). Statistical significance was determined by a Student's t test, 1-way ANOVA followed by multiparametric Dunnett's post-hoc test, or 2-way ANOVA. Differences were considered significant in instances where $p < 0.05$.

Supplemental Data

Supplemental Data including Figure S1 showing changes in mitochondrial morphology upon QD treatments and Figure S2 showing ROS formation in the presence of QDs, as revealed by enhanced nuclear staining with ethidium (red), and its reduction by NAC are available at http://www.chembiol.com/cgi/content/full/12/11/1227/DC1/.

Acknowledgments

This work was supported by the Juvenile Diabetes Research Foundation (Canada). We would like to thank J. Laliberté for assistance with confocal microscopy. J.L. would also like to thank R. Aikin for critically reviewing the manuscript.

Received: June 30, 2005
Revised: August 17, 2005
Accepted: September 8, 2005
Published: November 18, 2005

References

1. Michalet, X., Pinaud, F.F., Bentolila, L.A., Tsay, J.M., Doose, S., Li, J.J., Sundaresan, G., Wu, A.M., Gambhir, S.S., and Weiss, S. (2005). Quantum dots for live cells, in vivo imaging, and diagnostics. Science *307*, 538–544.
2. Medintz, I.L., Uyeda, H.T., Goldman, E.R., and Mattoussi, H. (2005). Quantum dot bioconjugates for imaging, labelling and sensing. Nat. Mater. *4*, 435–446.
3. Howarth, M., Takao, K., Hayashi, Y., and Ting, A.Y. (2005). Targeting quantum dots to surface proteins in living cells with biotin ligase. Proc. Natl. Acad. Sci. USA *102*, 7583–7588.
4. Wu, X., Liu, H., Liu, J., Haley, K.N., Treadway, J.A., Larson, J.P., Ge, N., Peale, F., and Bruchez, M.P. (2003). Immunofluorescent labeling of cancer marker Her2 and other cellular targets with semiconductor quantum dots. Nat. Biotechnol. *21*, 41–46.
5. Lidke, D.S., Nagy, P., Heintzmann, R., Arndt-Jovin, D.J., Post, J.N., Grecco, H.E., Jares-Erijman, E.A., and Jovin, T.M. (2004). Quantum dot ligands provide new insights into erbB/HER receptor-mediated signal transduction. Nat. Biotechnol. *22*, 198–203.
6. Dahan, M., Levi, S., Luccardini, C., Rostaing, P., Riveau, B., and Triller, A. (2003). Diffusion dynamics of glycine receptors revealed by single-quantum dot tracking. Science *302*, 442–445.
7. Stroh, M., Zimmer, J.P., Duda, D.G., Levchenko, T.S., Cohen, K.S., Brown, E.B., Scadden, D.T., Torchilin, V.P., Bawendi, M.G., Fukumura, D., et al. (2005). Quantum dots spectrally distinguish multiple species within the tumor milieu in vivo. Nat. Med. *11*, 678–682.
8. Larson, D.R., Zipfel, W.R., Williams, R.M., Clark, S.W., Bruchez, M.P., Wise, F.W., and Webb, W.W. (2003). Water-soluble quantum dots for multiphoton fluorescence imaging in vivo. Science *300*, 1434–1436.
9. Levene, M.J., Dombeck, D.A., Kasischke, K.A., Molloy, R.P., and Webb, W.W. (2004). In vivo multiphoton microscopy of deep brain tissue. J. Neurophysiol. *91*, 1908–1912.
10. Akerman, M.E., Chan, W.C.W., Laakkonen, P., Bhatia, S.N., and Ruoslahti, E. (2002). Nanocrystal targeting in vivo. Proc. Natl. Acad. Sci. USA *99*, 12617–12621.
11. Gao, X., Cui, Y., Levenson, R.M., Chung, L.W., and Nie, S. (2004). In vivo cancer targeting and imaging with semiconductor quantum dots. Nat. Biotechnol. *22*, 969–976.
12. Kim, S., Lim, Y.T., Soltesz, E.G., De Grand, A.M., Lee, J., Nakayama, A., Parker, J.A., Mihaljevic, T., Laurence, R.G., Dor, D.M., et al. (2004). Near-infrared fluorescent type II quantum dots for sentinel lymph node mapping. Nat. Biotechnol. *22*, 93–97.
13. Voura, E.B., Jaiswal, J.K., Mattoussi, H., and Simon, S.M. (2004). Tracking metastatic tumor cell extravasation with quantum dot nanocrystals and fluorescence emission-scanning microscopy. Nat. Med. *10*, 993–998.
14. Clapp, A.R., Medintz, I.L., Mauro, J.M., Fisher, B.R., Bawendi, M.G., and Mattoussi, H. (2004). Fluorescence resonance energy transfer between quantum dot donors and dye-labeled protein acceptors. J. Am. Chem. Soc. *126*, 301–310.
15. Medintz, I.L., Trammell, S.A., Mattoussi, H., and Mauro, J.M. (2004). Reversible modulation of quantum dot photoluminescence using a protein- bound photochromic fluorescence resonance energy transfer acceptor. J. Am. Chem. Soc. *126*, 30–31.
16. Bakalova, R., Ohba, H., Zhelev, Z., Ishikawa, M., and Baba, Y. (2004). Quantum dots as photosensitizers? Nat. Biotechnol. *22*, 1360–1361.
17. Samia, A.C., Chen, X., and Burda, C. (2003). Semiconductor quantum dots for photodynamic therapy. J. Am. Chem. Soc. *125*, 15736–15737.
18. Green, M., and Howman, E. (2005). Semiconductor quantum dots and free radical induced DNA nicking. Chem. Commun. (Camb.) 121–123.
19. Jaiswal, J.K., Mattoussi, H., Mauro, J.M., and Simon, S.M. (2003). Long-term multiple color imaging of live cells using quantum dot bioconjugates. Nat. Biotechnol. *21*, 47–51.
20. Dubertret, B., Skourides, P., Norris, D.J., Noireaux, V., Brivanlou, A.H., and Libchaber, A. (2002). In vivo imaging of quantum dots encapsulated in phospholipid micelles. Science *298*, 1759–1762.

21. Ballou, B., Lagerholm, B.C., Ernst, L.A., Bruchez, M.P., and Waggoner, A.S. (2004). Noninvasive imaging of quantum dots in mice. Bioconjug. Chem. *15*, 79–86.
22. Derfus, A.M., Chan, W.C.W., and Bhatia, S.N. (2004). Probing the cytotoxicity of semiconductor quantum dots. Nano Lett. *4*, 11–18.
23. Hoshino, A., Fujioka, K., Oku, T., Suga, M., Sasaki, Y.F., Ohta, T., Yasuhara, M., Suzuki, K., and Yamamoto, K. (2004). Physicochemical properties and cellular toxicity of nanocrystal quantum dots depend on their surface modification. Nano Lett. *4*, 2163–2169.
24. Kirchner, C., Liedl, T., Kudera, S., Pellegrino, T., Javier, A.M., Gaub, H.E., Stolzle, S., Fertig, N., and Parak, W.J. (2005). Cytotoxicity of colloidal CdSe and CdSe/ZnS nanoparticles. Nano Lett. *5*, 331–338.
25. Aldana, J., Wang, Y.A., and Peng, X.G. (2001). Photochemical instability of CdSe nanocrystals coated by hydrophilic thiols. J. Am. Chem. Soc. *123*, 8844–8850.
26. Aldana, J., Lavelle, N., Wang, Y.J., and Peng, X.G. (2005). Size-dependent dissociation pH of thiolate ligands from cadmium chalcogenide nanocrystals. J. Am. Chem. Soc. *127*, 2496–2504.
27. Shiohara, A., Hoshino, A., Hanaki, K., Suzuki, K., and Yamamoto, K. (2004). On the cyto-toxicity caused by quantum dots. Microbiol. Immunol. *48*, 669–675.
28. Lovric, J., Bazzi, H.S., Cuie, Y., Fortin, G.R.A., Winnik, F.M., and Maysinger, D. (2005). Differences in subcellular distribution and toxicity of green and red emitting CdTe quantum dots. J. Mol. Med. *83*, 377–385.
29. Ferri, K.F., and Kroemer, G. (2001). Organelle-specific initiation of cell death pathways. Nat. Cell Biol. *3*, E255–E263.
30. Karbowski, M., and Youle, R.J. (2003). Dynamics of mitochondrial morphology in healthy cells and during apoptosis. Cell Death Differ. *10*, 870–880.
31. Leist, M., and Jaattela, M. (2001). Four deaths and a funeral: from caspases to alternative mechanisms. Nat. Rev. Mol. Cell Biol. *2*, 589–598.
32. Riedl, S.J., and Shi, Y. (2004). Molecular mechanisms of caspase regulation during apoptosis. Nat. Rev. Mol. Cell Biol. *5*, 897–907.
33. Liang, Y., Yan, C., and Schor, N.F. (2001). Apoptosis in the absence of caspase 3. Oncogene *20*, 6570–6578.
34. Porter, A.G. (1999). Protein translocation in apoptosis. Trends Cell Biol. *9*, 394–401.
35. Li, P., Nijhawan, D., Budihardjo, I., Srinivasula, S.M., Ahmad, M., Alnemri, E.S., and Wang, X.D. (1997). Cytochrome c and dATP-dependent formation of Apaf-1/caspase-9 complex initiates an apoptotic protease cascade. Cell *91*, 479–489.
36. Wei, M.C., Zong, W.X., Cheng, E.H.Y., Lindsten, T., Panoutsakopoulou, V., Ross, A.J., Roth, K.A., MacCregor, G.R., Thompson, C.B., and Korsmeyer, S.J. (2001). Proapoptotic BAX and BAK: a requisite gateway to mitochondrial dysfunction and death. Science *292*, 727–730.
37. Luetjens, C.M., Kogel, D., Reimertz, C., Dussmann, H., Renz, A., Schulze-Osthoff, K., Nieminen, A.L., Poppe, M., and Prehn, J.H. (2001). Multiple kinetics of mitochondrial cytochrome c release in drug-induced apoptosis. Mol. Pharmacol. *60*, 1008–1019.
38. Gaponik, N., Talapin, D.V., Rogach, A.L., Hoppe, K., Shevchenko, E.V., Kornowski, A., Eychmuller, A., and Weller, H. (2002). Thiol-capping of CdTe nanocrystals: an alternative to organometallic synthetic routes. J. Phys. Chem. B *106*, 7177–7185.
39. Haga, N., Fujita, N., and Tsuruo, T. (2003). Mitochondrial aggregation precedes cytochrome c release from mitochondria during apoptosis. Oncogene *22*, 5579–5585.
40. Janicke, R.U., Sprengart, M.L., Wati, M.R., and Porter, A.G. (1998). Caspase-3 is required for DNA fragmentation and morphological changes associated with apoptosis. J. Biol. Chem. *273*, 9357–9360.
41. Borner, C., and Monney, L. (1999). Apoptosis without caspases: an inefficient molecular guillotine? Cell Death Differ. *6*, 497–507.
42. Vercammen, D., Brouckaert, G., Denecker, G., Van de Craen, M., Declercq, W., Fiers, W., and Vandenabeele, P. (1998). Dual signaling of the Fas receptor: initiation of both apoptotic and necrotic cell death pathways. J. Exp. Med. *188*, 919–930.
43. Nicotera, P., Leist, M., and Manzo, L. (1999). Neuronal cell death: a demise with different shapes. Trends Pharmacol. Sci. *20*, 46–51.
44. Finkel, T., and Holbrook, N.J. (2000). Oxidants, oxidative stress and the biology of ageing. Nature *408*, 239–247.
45. Prestwich, E.G., Roy, M.D., Rego, J., and Kelley, S.O. (2005). Oxidative DNA strand scission induced by peptides. Chem. Biol. *12*, 695–701.
46. Oberdorster, E. (2004). Manufactured nanomaterials (fullerenes, C60) induce oxidative stress in the brain of juvenile largemouth bass. Environ. Health Perspect. *112*, 1058–1062.
47. Cotgreave, I.A. (1997). N-acetylcysteine: pharmacological considerations and experimental and clinical applications. Adv. Pharmacol. *38*, 205–227.
48. Cooper, A.J., and Kristal, B.S. (1997). Multiple roles of glutathione in the central nervous system. Biol. Chem. *378*, 793–802.
49. Ratan, R.R., Murphy, T.H., and Baraban, J.M. (1994). Oxidative stress induces apoptosis in embryonic cortical-neurons. J. Neurochem. *62*, 376–379.
50. Heales, S.J., Bolanos, J.P., Stewart, V.C., Brookes, P.S., Land, J.M., and Clark, J.B. (1999). Nitric oxide, mitochondria and neurological disease. Biochim. Biophys. Acta *1410*, 215–228.
51. Newmeyer, D.D., and Ferguson-Miller, S. (2003). Mitochondria: releasing power for life and unleashing the machineries of death. Cell *112*, 481–490.
52. Shidoji, Y., Hayashi, K., Komura, S., Ohishi, N., and Yagi, K. (1999). Loss of molecular interaction between cytochrome c and cardiolipin due to lipid peroxidation. Biochem. Biophys. Res. Commun. *264*, 343–347.
53. McStay, G.P., Clarke, S.J., and Halestrap, A.P. (2002). Role of critical thiol groups on the matrix surface of the adenine nucleotide translocase in the mechanism of the mitochondrial permeability transition pore. Biochem. J. *367*, 541–548.
54. Madesh, M., and Hajnoczky, G. (2001). VDAC-dependent permeabilization of the outer mitochondrial membrane by superoxide induces rapid and massive cytochrome c release. J. Cell Biol. *155*, 1003–1015.